Journal of Sound and Vibration (2002) **253**(2), 401–419
doi:10.1006/jsvi.2001.4061 available online at http://www.idealibrary.com on IDEAL®

SOUND RADIATION FROM A VIBRATING RAILWAY WHEEL

D. J. Thompson and C. J. C. Jones

Institute of Sound and Vibration Research, University of Southampton, Highfield, Southampton SO17 1BJ, England.
E-mail: djt@isvr.soton.ac.uk

(*Received* 29 *May* 2001, *and in final form* 1 *October* 2001)

The sound radiation characteristics of a railway wheel are investigated by using boundary element calculations. The axisymmetry of the wheel allows an axi-harmonic formulation to be used, in which the wheel is defined by a two-dimensional mesh of its cross-section and the motion is decomposed into harmonics of different numbers of nodal diameters. The radiation ratios of the wheel, vibrating in its various normal modes, are calculated for a range of frequencies. The effects of variation in the wheel radius, web thickness and tyre depth are also investigated. From these results, simple formulae are proposed that allow the radiation ratios to be approximated closely. These are more convenient than the boundary element calculations for calculating the rolling noise from a wheel since they are a function of a few simple geometrical parameters. The directivity of wheel radiation is also considered, with comparisons with measured data indicating that simple monopole and dipole characteristics can be applied.

1. INTRODUCTION

Wheel/rail rolling noise is usually the most important source of environmental noise from railways at conventional speeds. It is radiated by vibrations of the wheels, rails and sleepers excited by the roughness of the wheel and rail running surfaces [1]. Since the 1970s theoretical models have been developed to predict the generation of rolling noise [2–6]. These models are composed of dynamic models for the wheel and the track, an interaction model based on their frequency response functions and separate models for their noise radiation. This paper focuses, for the particular case of a wheel, on the latter aspect: the noise radiation due to a given vibration level and distribution.

In order to describe the acoustic radiation from a vibrating structure, two quantities may be defined. The first quantity is the radiation ratio, or radiation efficiency. This is the sound power produced by a vibrating structure, normalized by the sound power that would be radiated by the same mean square spatially averaged velocity if the surface were part of an infinite plane, all vibrating in phase. The radiation ratio of a vibrating structure is generally small at low frequencies and tends to 1 at high frequencies. The transition between these two regimes depends on the size of the structure and on the structural wavelength, each seen in comparison with the acoustic wavelength.

The second quantity required to describe the acoustic radiation is the directivity. This is a measure of the spatial distribution of the sound field, and allows the sound pressure at a receiver point in the far field to be derived from the sound power.

0022-460X/02/$35.00

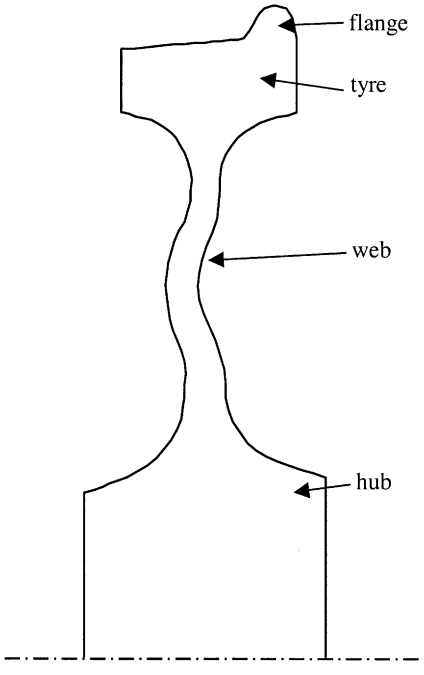

Figure 1. Cross-section of UIC 920 mm freight wheel.

Most railway wheels are axisymmetric. The cross-section of a standard UIC freight wheel with a diameter of 0.92 m is shown in Figure 1. The axle is not shown. The tyre region, that runs on the rail, usually has an overall width of 135 mm including the flange, whereas the thinner web region, connecting the tyre to the hub, is more typically 20–25 mm wide at its narrowest point. Due to its light damping, the vibration of the wheel is dominated by its normal modes. The axisymmetric geometry results in modes that can be defined by the number of node lines running radially across the wheel (nodal diameters) and the number of node lines that run circumferentially around the wheel (nodal circles) [7]. Examples of modes with two nodal diameters are shown schematically in Figure 2. These are a 0-nodal-circle axial mode in which the amplitude increases to a maximum at the tread, a radial mode and a 1-nodal-circle mode where the web region moves out of phase with the tread.

Previously, models of the sound radiation from railway wheels have made use of the Rayleigh integral technique [8]. In this, a vibrating surface is visualized as part of an infinite flat surface and the sound pressure at any location is found by integrating the contribution from each part of the surface. Such a technique has been used successfully in determining the radiation ratio of rectangular flat plates [9, 10]. It does not take into account any interaction between the sound field generated by the front and rear of the structure, nor the effect of complex geometrical shape. Nevertheless, it has also been used to predict the sound radiated by a railway wheel [11, 12].

Fingberg [13] used the boundary element (BE) method to predict the sound radiation from wheels. This is a numerical technique in which the vibrating surface is represented by a mesh of elements and the sound field is calculated by solving the Helmholtz integral equation in discrete form. Making use of the axisymmetry of the wheel, Fingberg developed a model in which the wheel is represented only by its cross-section. He showed that the radiation ratio can differ significantly at low frequencies from that predicted by

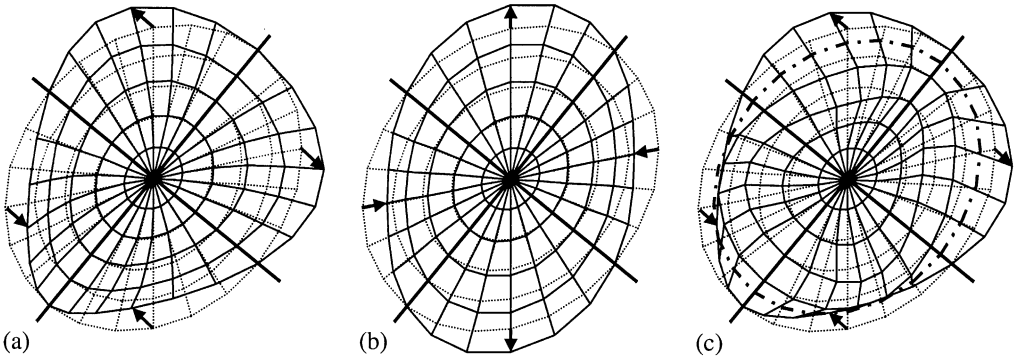

Figure 2. Idealization of wheel modes with 2 nodal diameters. (a) 0-nodal-circle axial mode, (b) radial mode, (c) 1-nodal-circle axial mode. Thick solid lines indicate nodal diameters, thick chain line indicates nodal circle and arrows indicate direction of motion at anti-nodes.

the Rayleigh integral method, whereas at high frequencies variations of around 2 dB were found. Experimental validation was performed on a model wheel to scale 1 : 5.

The boundary element method is computationally intensive and requires a considerable amount of input data to define the wheel geometry and its vibration. For use in predicting rolling noise, therefore, it is preferable to be able to use simpler models, the input parameters for which should ideally be limited to features such as the wheel radius, width, etc.

In this paper, boundary element predictions are presented of the radiation ratio of a wheel vibrating in its various natural modes. By varying the wheel radius and web geometry the dependence on various parameters is obtained. From this a series of simple formulae are derived that can be implemented into a wheel/rail noise prediction model. The directivity of wheel radiation is also considered, with comparisons given with measured data.

2. PREDICTIONS OF THE RADIATION RATIO OF A WHEEL

2.1. METHOD

Boundary element predictions have been made using an "axi-harmonic" option within a standard software package. This allows an axisymmetric structure to be modelled with non-axisymmetric boundary conditions, using a Fourier series expansion [14]. Since the vibration of a wheel is dominated by its modes, the sound radiation has been calculated for each individual wheel mode in the range of interest. These mode shapes have a dependence on the circumferential angle θ of $\cos n\theta$ or $\sin n\theta$, where n is the number of nodal diameters in the mode shape. Thus they correspond to a single Fourier component in the axi-harmonic decomposition of the boundary conditions.

The modes of vibration of a wheel were calculated first by using a finite element package. In this model the wheel is represented by its cross-section and modes with each circumferential order, n, are calculated. The wheel vibration has been calculated without the axle present, but instead a rigid constraint was applied at the inner edge of the hub. This gives a very good approximation to the modes of a wheel with $n \geqslant 2$, which are the most important modes for rolling noise generation [7]. In practice, the modes with $n = 0$ are coupled to extension of the axle and those with $n = 1$ are coupled to flexure of the axle [7] but this is not considered here.

Although a mode of the wheel occurs at a single frequency, the radiated sound power W_{rad} due to this mode shape has been calculated for a range of frequencies for each mode. This can then be used to derive the radiation ratio σ for this mode shape by using the definition

$$\sigma = W_{rad}/\rho_0 c_0 S\langle\overline{v^2}\rangle, \tag{1}$$

where ρ_0 is the density of air, c_0 is the speed of sound in air, S is the surface area of the structure and v^2 is the squared normal velocity of the surface, which is both temporally ($\overline{\ }$) and spatially ($\langle\ \rangle$) averaged.

The hole left in the hub in the finite element mesh had to be closed by using additional boundary elements with zero vibration amplitude (see Figure 1). By this means, acoustic leakage through this hole, which would not be present in reality due to the presence of the axle, was prevented.

The formulation used in the boundary element analyses is based upon the indirect boundary element method [15]. Rather than use the sound pressures and velocities calculated at the wheel surface, it was found that results for the radiated sound power could be calculated more stably by integration of the mean square pressure amplitude over a spherical field point mesh Γ situated in the far field

$$W_{rad} = \int_\Gamma \frac{\overline{p^2}}{\rho_0 c_0}\,\mathrm{d}\Gamma. \tag{2}$$

Predictions were carried out for 100 logarithmically spaced frequency steps between 50 and 6000 Hz. The well-known problem in the boundary element method whereby frequencies exist at which the solution is "non-unique" [15] was encountered at only one or two frequencies for each wheel. It was found that a satisfactory approach to dealing with this was to identify these frequencies and to omit the results affected.

2.2. RESULTS FOR VARIOUS MODE TYPES

The modes of vibration of a wheel have been described in detail in references [1, 7]. The main modes are axial (out of plane), although radial (in plane) motion is also important. Each mode type occurs with $n = 0, 1, 2, 3, \ldots$ nodal diameters. The 920 mm diameter wheel shown in Figure 1 has been taken as a reference wheel. The deformation of the cross-section of this wheel is presented in Figure 3 for various modes with $n = 2$. The simplest wheel modes to visualize are the axial modes with no nodal circle (Figure 3(a)). In this case the amplitude on an anti-nodal plane increases from the hub to its maximum at the perimeter. The predominantly radial modes (Figure 3(b)), and the 1-nodal-circle axial modes (Figure 3(c)), both contain coupled axial and radial motion due to the asymmetric wheel web [7]. These various mode shapes are used as velocity boundary conditions in the boundary element calculation.

The radiation ratio obtained for the 0-nodal-circle axial mode shapes is shown in Figure 4(a). In each case, the radiation ratio rises sharply at low frequency, reaching a value of 1 between about 250 and 1250 Hz, and then oscillating slightly around the value of 1. The frequency at which σ becomes equal to 1 increases as n is increased. Moreover, the slope of the low-frequency part of the curve increases with increasing n. It is found to correspond to a dependence on frequency, f, of f^4 for $n = 0$, f^6 for $n = 1$, f^8 for $n = 2$, etc. The mode with $n = 0$ in this case corresponds to an axial oscillation of the whole tyre in phase, and can thus be represented by a dipole at low frequencies, where the dimensions of the wheel are small compared to the acoustic wavelength. The mode with $n = 1$ has areas on opposite sides of the wheel face that are oscillating out of phase. This may therefore be

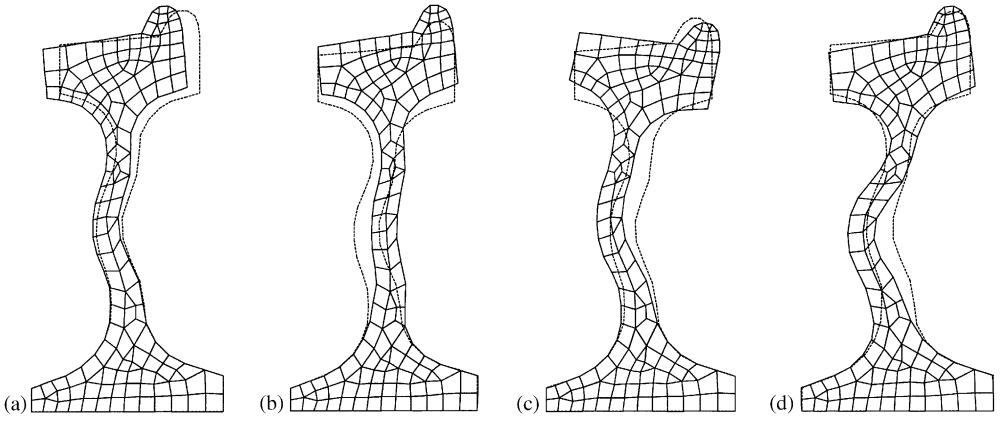

Figure 3. Modes of UIC 920 mm freight wheel with $n=2$. (a) 0-nodal-circle axial mode at 351 Hz, (b) predominantly radial mode at 1670 Hz, (c) 1-nodal-circle axial mode at 2280 Hz, (d) 2-nodal-circle axial mode at 3850 Hz.Undeformed shape shown dotted.

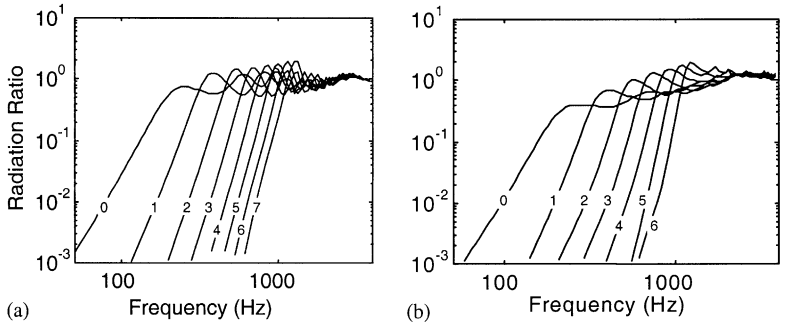

Figure 4. Radiation ratio of various axial modes of 920 mm freight wheel with various numbers of nodal diameters, n. (a) 0-nodal-circle axial modes, (b) 1-nodal-circle axial modes.

seen to approximate to two dipoles out of phase, i.e., a quadrupole source, at low frequencies. The frequency dependence of the radiation ratio for these modes is therefore explained in terms of the characteristic frequency dependence of simple sources. Modes with higher values of n correspond to higher order multipoles.

Figure 4(b) shows equivalent results for 1-nodal-circle axial modes. In these mode shapes, the tyre region rotates, while the maximum axial motion is in the web region. The results are very similar to those for the 0-nodal-circle axial modes, indicating that the number of nodal diameters, n, is more important than the deformed shape of the cross-section.

The predominantly radial modes of this wheel are found to contain considerable axial motion, similar in form to the 1-nodal-circle modes; see Figure 3. Their radiation ratios are therefore rather complex, and it is more instructive to consider the radiation ratio of a purely radial motion of the tyre. The web is assumed not to vibrate. The result is shown in Figure 5. Here the radiation ratio does not reach 1 until close to 1 kHz. At very low frequencies the slope of the curves is less than those in Figure 4. It is found to correspond to f^2 for $n=0$, f^4 for $n=1$, f^6 for $n=2$, etc. The mode with $n=0$ corresponds to a radial pulsation of the whole tyre in phase, and can thus be represented by a monopole at low

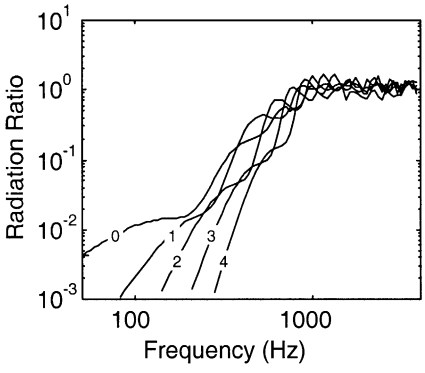

Figure 5. Radiation ratio of radial motion of the tyre of 920 mm freight wheel with various numbers of nodal diameters, n.

frequencies. In the mode with $n=1$, the tyre oscillates and thus corresponds to a dipole at low frequencies. For each value of n, the order of the multipole approximation at low frequency is one less than for the corresponding axial motion.

2.3. COMPARISONS WITH MEASUREMENT RESULTS

Measurement data of the radiation ratio of a UIC 920 mm wheel has been obtained by TNO [16]. The wheel, attached to its axle, was located in a semi-anechoic room and excited by a shaker attached to the web. The acceleration was measured at 8 positions on a single cross-section directly opposite the excitation point, and therefore on an anti-nodal plane. The sound power was measured using intensity scans of a number of areas, which together completely enclosed the wheel. The radiation ratio was obtained according to equation (1) for each mode, but of course only at its natural frequency.

The results from these measurements are shown in Figure 6 in the form of a radiation index ($10\log_{10}\sigma$). At high frequencies the average result is $+3$ dB, indicating a possible calibration error, although extensive investigation failed to locate this. Compared to this high-frequency asymptote, the three results below 1 kHz are the most noteworthy. The $n=0$ axial mode at 290 Hz has a radiation ratio similar to the high-frequency results; according to the predictions in Figure 4(a), this mode has its natural frequency at the first peak of the radiation ratio curve, at a value just below 1. The $n=2$ axial mode at 370 Hz is about 10 dB below the high-frequency results, which is entirely consistent with Figure 4(a). The $n=3$ axial mode at 920 Hz is 3 dB below the high-frequency results. In the predictions, this frequency corresponds to the first dip in the curve at which σ drops to about 0.5.

Hence, apart from the unexplained 3 dB shift in all the results, the measurements confirm the predictions. They also show that, for most modes of an actual wheel, the natural frequencies occur in the region where the radiation ratio is close to 1.

3. DEPENDENCE ON WHEEL GEOMETRY

3.1. EFFECT OF WHEEL RADIUS

In this section the radiation ratios of the various modes of a wheel are compared for a set of notional wheels of different radii. These are wheels shown in Figure 7, from which it can be seen that the tyre and hub regions are similar to the wheel in Figure 1, whereas the

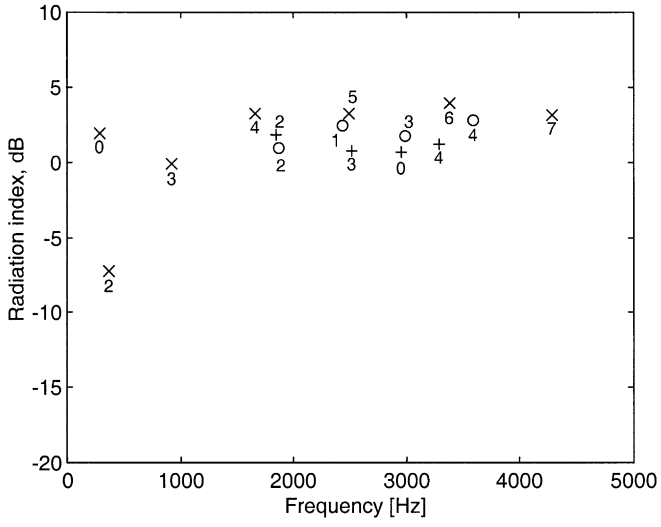

Figure 6. Measured radiation index of various axial modes of 920 mm freight wheel. ×, 0-nodal-circle axial modes; +, radial modes, o, 1-nodal-circle axial modes. Numbers of nodal diameters, n, are indicated against each point [16].

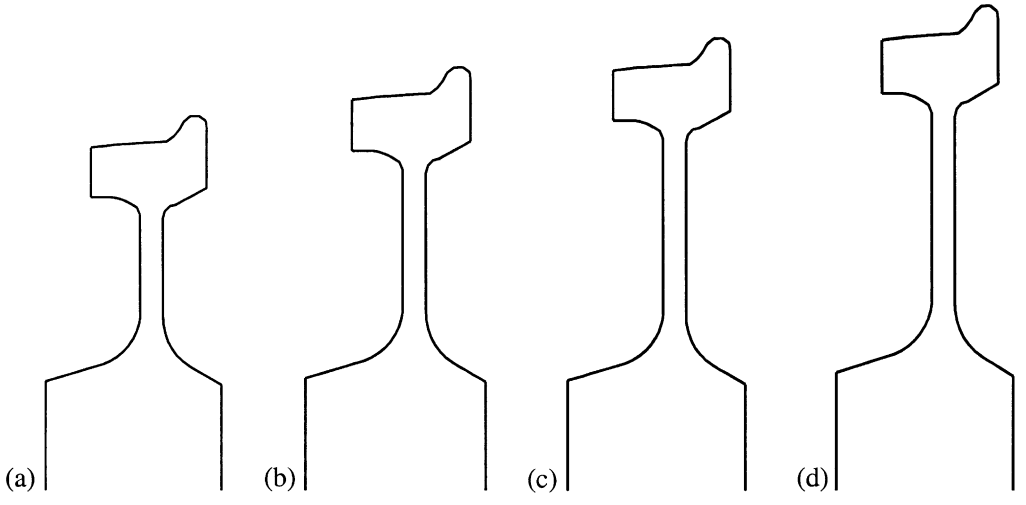

Figure 7. Notional wheel cross-sections used for studying the effect of wheel radius. (a) 0.38 m, (b) 0.42 m, (c) 0.46 m, (d) 0.50 m.

web is straight and of variable length. In each case, the modes of vibration of the wheels in question have been calculated and assigned as the boundary conditions in the boundary element calculation.

For a reduction in wheel radius it is found that the radiation ratio curves are similar, but are shifted to the right. Figure 8 shows the results for 0-nodal-circle axial modes from all four radii, together with that for the reference wheel. These are plotted against frequency normalized by the ratio of the wheel radius, r, to the reference value, $r_0 = 0{\cdot}46$ m. It can be seen that all the results collapse onto a single curve for a given value of n. A fitted curve is

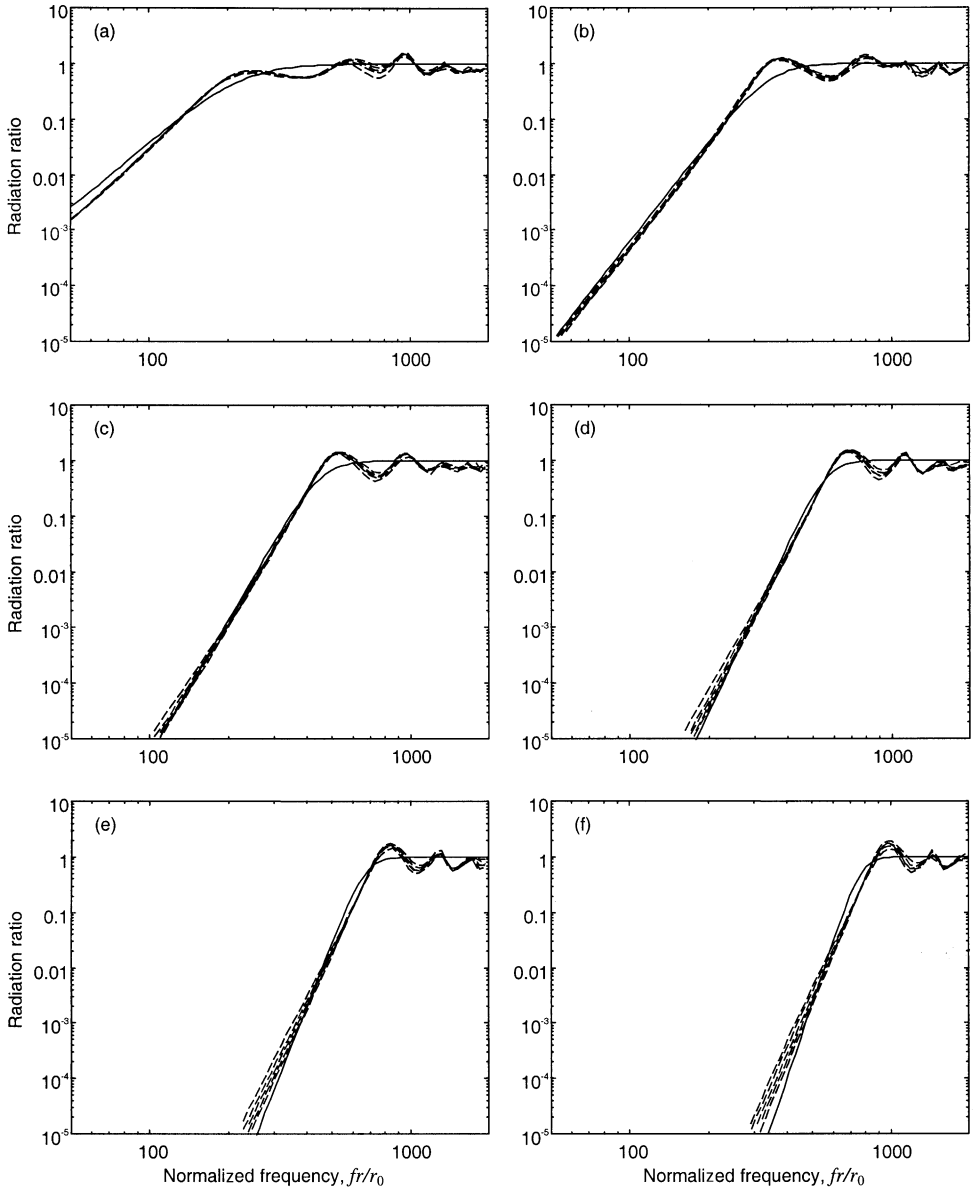

Figure 8. Radiation ratios of 0-nodal-circle axial modes for five wheels of different radii. (a) $n=0$, (b) $n=1$, (c) $n=2$, (d) $n=3$, (e) $n=4$, (f) $n=5$. – – –, predictions for each wheel; ——, curve fit.

also shown in this figure; it will be discussed in section 4 below. Similar results are also found for the 1-nodal-circle modes.

In Figure 9, the radiation ratio for radial motion of the tyre is shown for wheels of different radii. In this case the frequency is normalized by $(r/r_0)^{1/2}$. Again similar features are seen in each case, although the results for the reference wheel differ somewhat from those for the straight webbed wheels, particularly for $n=0$ and 1. Again a fitted curve is shown that will be described in section 4.

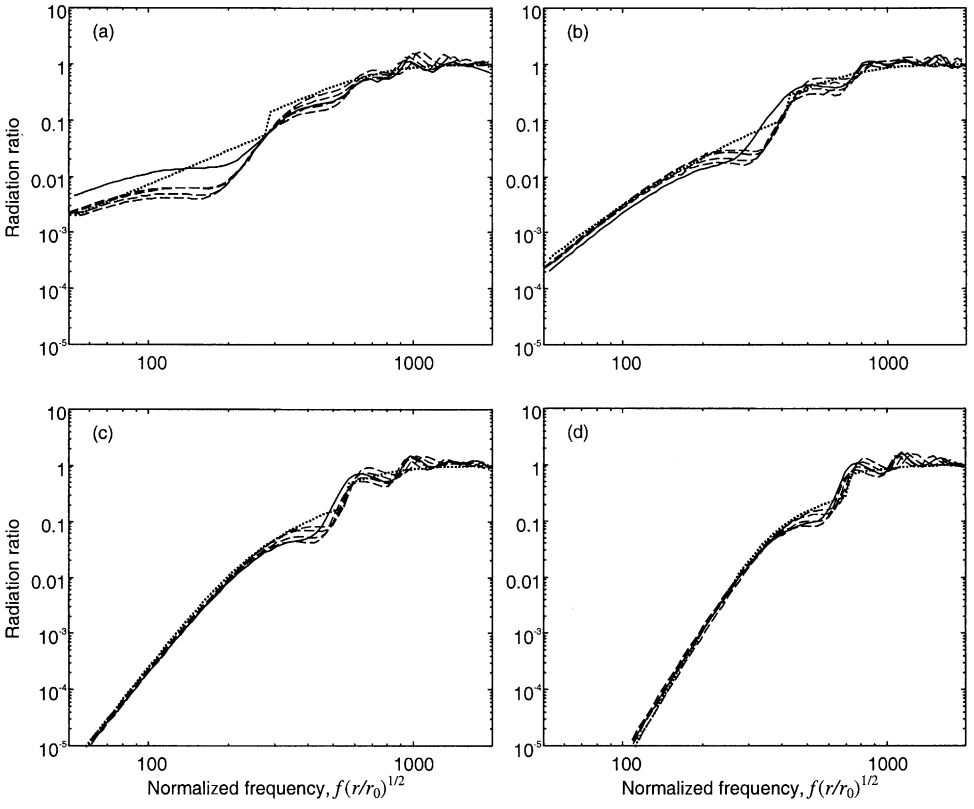

Figure 9. Radiation ratios of radial motion for five wheels of different radii. (a) $n=0$, (b) $n=1$, (c) $n=2$, (d) $n=3$. - - -, predictions for each straight-webbed wheel; ——, prediction for reference wheel; ·····, curve fit.

3.2. EFFECT OF WEB SHAPE

The shape of the wheel web was found to have no significant effect on the results for axial motion, but it has considerable effect on those for radial motion. To demonstrate this, a number of notional wheels have been considered, shown in Figure 10. These wheels all have a radius of 0·42 m, and are compared with wheel (b) from Figure 7, referred to as a "normal" wheel. The hub and running surface is kept constant in each case but the web width and the tyre depth are varied.

The radiation ratios for radial motion of the tyre are shown in Figure 11 for the wheel with the solid web, i.e., wheel (b) in Figure 10. The motion here is thus only on the outer surface of the tyre. From the high-frequency asymptote of 1, these curves begin to drop just below 1 kHz in all cases, with a slope of f^2. A further steepening of the gradient occurs at a lower frequency that depends on n.

In Figure 12, the results for the various notional wheel designs are compared for each value of n. The largest differences occur for $n=0$. The highest radiation ratio at low frequencies occurs for the wheel with the solid web. For the other wheels, partial cancellation occurs between the acoustic sources corresponding to motion of the outer and inner surfaces of the tyre. If the two surface areas were equal, this cancellation would leave a dipole-type radiation at the tyre. However, since the areas cannot be equal, a residual monopole component remains which dominates the low-frequency behaviour. As the web

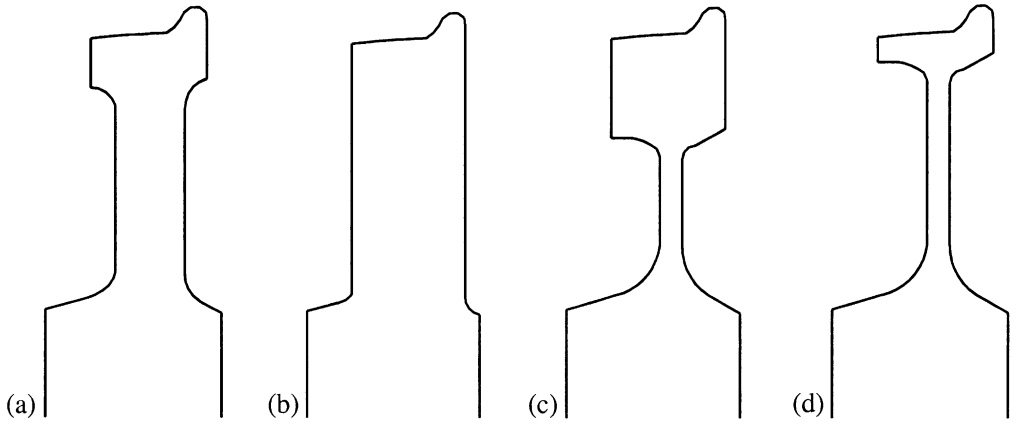

Figure 10. Notional wheel cross-sections used for studying the effect of wheel web shape, each of radius 0·42 m. (a) wide web, (b) solid web, (c) double thickness tyre, (d) half-thickness tyre.

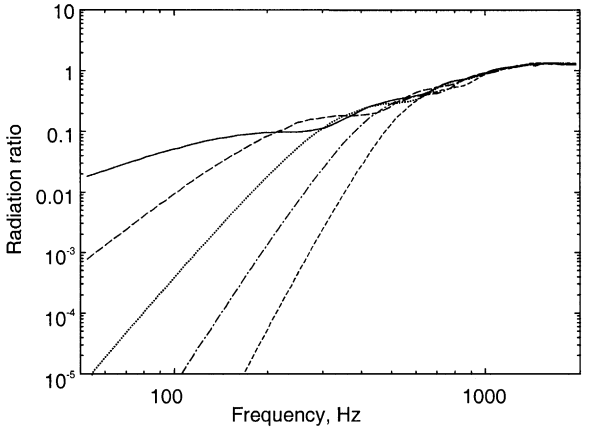

Figure 11. Radiation ratios of radial motion for wheel with solid web and radius 0·42 m. ——, $n=0$; – – –, $n=1$; ·····, $n=2$; – · – ·, $n=3$; - - -, $n=4$.

or the tyre are made thinner, the low-frequency monopole component is reduced in magnitude.

Similar trends, though to a smaller degree, are found in the results for the modes with $n \geqslant 1$. As the number of nodal diameters increases, the effect of the web and tyre geometry becomes smaller.

4. APPROXIMATE FORMULAE

4.1. AXIAL MOTION

In this section, simple formulae are sought that will describe the radiation ratios obtained above by using boundary element predictions. The radiation ratios for axial motion have been seen to have the form of a multipole, with a low-frequency slope corresponding to f^{2n+4} and these frequency dependences have been related to a physical

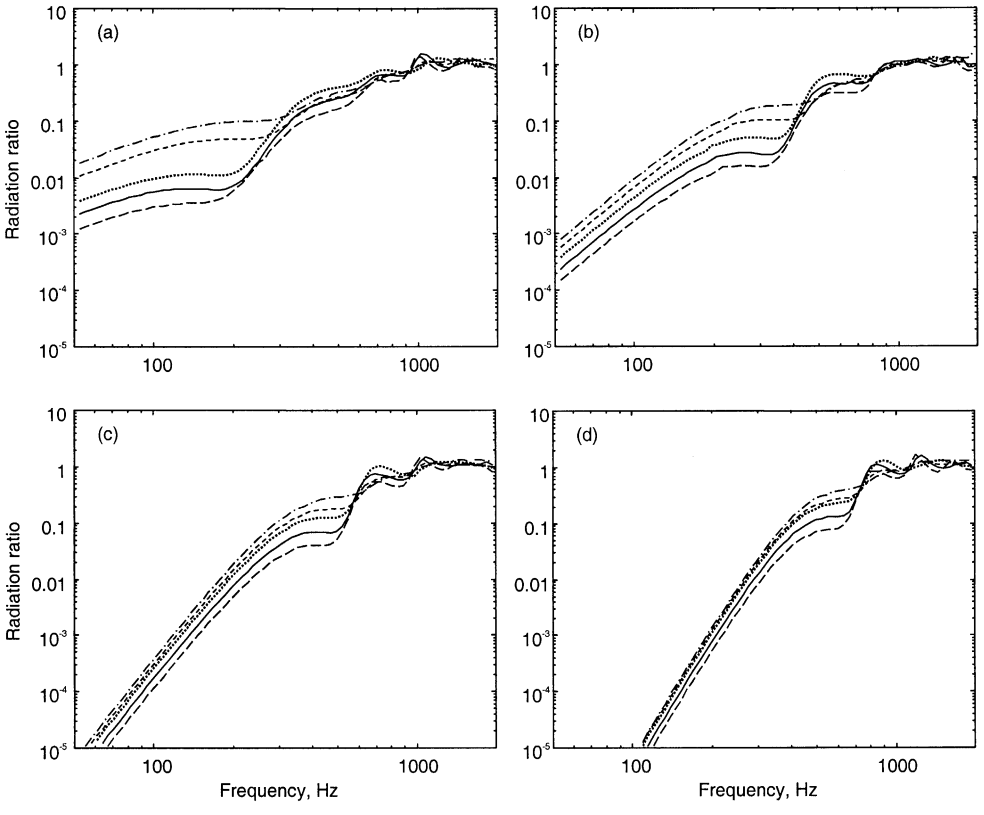

Figure 12. Radiation ratios of radial motion for various straight-webbed wheels with radius 0.42 m. ——, normal wheel; – – –, double thickness tyre; ····· half-thickness tyre; – · – ·, solid web; - - - wide web. (a) $n=0$, (b) $n=1$, (c) $n=2$, (d) $n=3$.

explanation in terms of simple source approximations. A suitable function to fit such a curve is

$$\sigma_a(n) = \frac{1}{1+(f_{ca}(n)/f)^{2n+4}}, \tag{3}$$

where σ_a is the radiation ratio for axial motion and f_{ca} is a transition frequency for axial motion, both being dependent on n. It has been seen in Figure 8 that f_{ca} is inversely proportional to the radius of the wheel. The value of f_{ca} has been determined by fitting a curve of the form of equation (3) to the results, as in Figure 8, with f_{ca} selected according to

$$f_{ca}(n) = c_0\mu/2\pi r, \tag{4}$$

where μ is a scaling parameter that has been varied. In determining the optimum value of μ, the frequency range considered has been limited to frequencies below 2000 Hz, as the high-frequency part of the curves is not affected by the choice of μ. Moreover, frequencies at which $\sigma < 10^{-3}$ were also omitted, as smaller values do not contribute significantly to the overall noise level, and inaccuracies can be introduced through the numerical integration of equation (2). The dB error in the radiation ratio has been determined at each calculation frequency within this range and for each wheel. The value of μ that minimizes the mean square error has then been chosen as the most suitable one. This is shown in

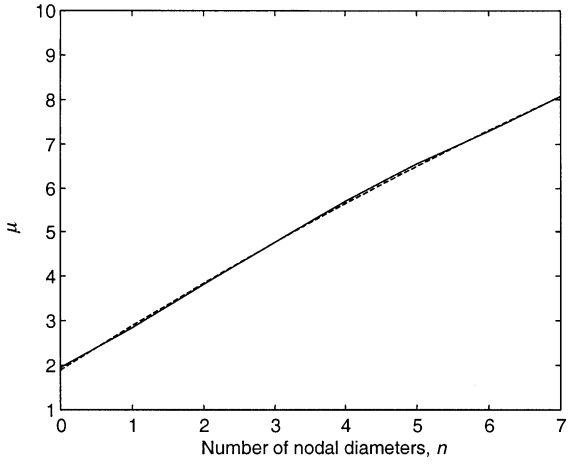

Figure 13. Factor μ used for determining transition frequency f_{ca} for axial motion, see equation (4). ——, found by minimizing r.m.s. error in radiation ratio; - - -, from curve fit, equation (5).

Figure 13, along with a simple curve fit to this value of μ as a function of n, given by

$$\mu = 1{\cdot}90 + 1{\cdot}015n - 0{\cdot}0189n^2. \tag{5}$$

Figure 14 shows the mean and r.m.s. differences between the boundary element results and the radiation ratios calculated using equations (3–5). The mean error indicates any bias in the curve which is small, whereas the r.m.s. error indicates the amount of fluctuation of the BE results around the approximate results. The corresponding radiation ratios predicted by equations (3–5) are included in Figure 8. Clearly these curves are a compromise. While missing some of the detailed shape of the BE curves, particularly the oscillation around 1, the overall form is reproduced well. The r.m.s. error increases with higher values of n. In practice, this is due to the region below f_{ca}, whereas the natural frequencies of modes with $n > 3$ will be well above the corresponding value of f_{ca}, so that $\sigma \approx 1$.

4.2. RADIAL MOTION

The corresponding exercise of deriving simple formulae for radial motion is slightly more complex. The slope of the curves in Figures 5, 9 and 11 has been seen to follow f^{2n+2} at low frequencies while the dependence on wheel radius has already been shown to be of the form $r^{-1/2}$. There will also be a dependence on the tyre width, but since this parameter does not vary significantly for real wheels, it is not investigated further here.

It is instructive to begin with the wheel with the solid web, as here no cancellation occurs between inner and outer tyre and therefore the curves are simpler. Based on the slope noted above and the structure of two transition frequencies, the proposed model is

$$\sigma_r(n) = \frac{1}{1 + (f_{r2}(n)/f)^2} \quad \text{for } n = 0, \tag{6a}$$

$$\sigma_r(n) = \frac{1}{1 + (f_{r1}(n)/f)^{2n}} \times \frac{1}{1 + (f_{r2}(n)/f)^2} \quad \text{for } n > 0, \tag{6b}$$

where $f_{r1} = 120n$ and $f_{r2} = 800$ Hz in this case ($r = 0{\cdot}42$ m). The first of these is related to the wavelength in the wheel tyre whereas the second depends only on the wheel geometry.

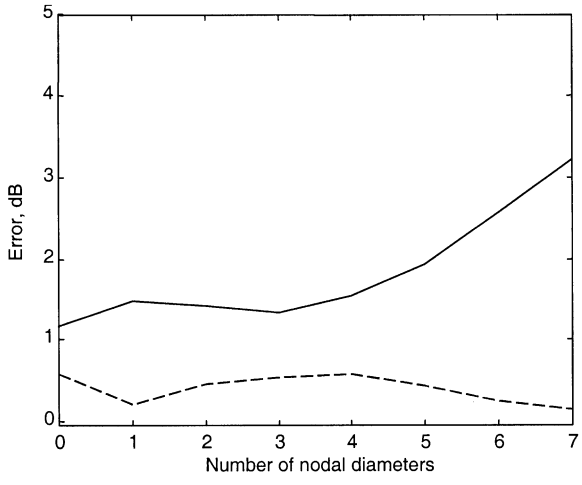

Figure 14. Error in radiation index of axial 0-nodal-circle modes if equations (3–5) are used. ——, r.m.s. error for all frequency points in range, – – –, mean error.

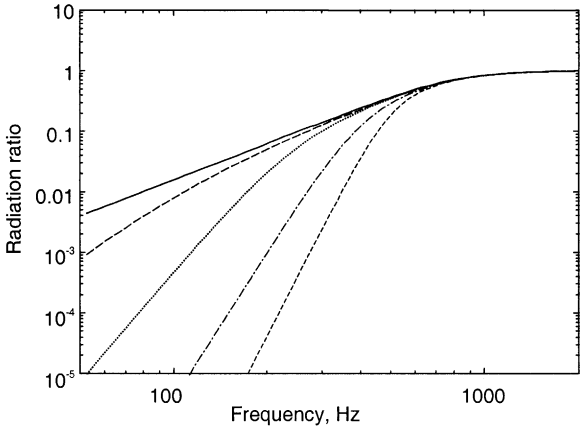

Figure 15. Approximate radiation ratios of radial motion for wheel with solid web and radius 0.42 m from equations (6). ——, $n=0$; – – –, $n=1$; ····· $n=2$; – · – ·, $n=3$; - - - $n=4$.

Equation (6b) implies a frequency dependence of f^{2n+2} for $f \ll f_{r1}$ and f^2 in the intermediate frequency range $f_{r1} < f < f_{r2}$.

The results of this model are shown in Figure 15. By comparing this to Figure 11, it can be seen that the results for $n > 0$ agree quite closely with the BE results. The results for $n = 0$ show a discrepancy of about a factor of 4 below 200 Hz, where the BE results rise above those of equation (6a). However, since no significant $n = 0$ radial motion occurs in practice below 1 kHz (the relevant mode of vibration occurs at about 3 kHz), this discrepancy is considered acceptable.

The next step is to consider the various wheels with different web and tyre dimensions. The BE predictions were shown in Figure 12. At high frequencies, the results follow closely those for the solid web (Figure 11) and equations (6) can be used to model these curves. However, at low frequencies, the radiation ratio drops by an amount that differs between wheels. It may be supposed that the magnitude of this drop is dependent

on the ratio of the areas

$$\gamma = (S_{out} - S_{in})/(S_{out} + S_{in}), \tag{7}$$

where S_{out} is the area of the outer surface of the tyre (the tread) and S_{in} is the area of the inner surfaces of the tyre. Thus the total area of the tyre active in radial motion is $S_{out} + S_{in}$. At low frequencies, cancellation between the radiation from the inner and outer surfaces leaves a residual area of $S_{out} - S_{in}$. The frequency below which the radiation ratio drops is found to be given approximately by

$$f_{r3} = 280 + 150n \tag{8}$$

for this wheel radius. For frequencies below f_{r3} it is found that the radiation ratio is reduced from that given by equations (6) by a factor of approximately $\sqrt{\gamma}$. The resulting predictions are given in Figure 16 which may be compared with the BE results of Figure 12. Using this factor works well for $n \geqslant 2$. For $n = 0$ the factor should be nearer to γ but, as noted above, the prediction for the solid-webbed wheel is less accurate anyway at $n = 0$; see also Figure 9(a). In any case, the results are unlikely to be significant as $n = 0$ radial motion does not occur at low frequencies. For $n = 1$ the simple model gives a slight over-prediction at low frequencies for the normal and thin-tyred wheels; see also Figure 9(b).

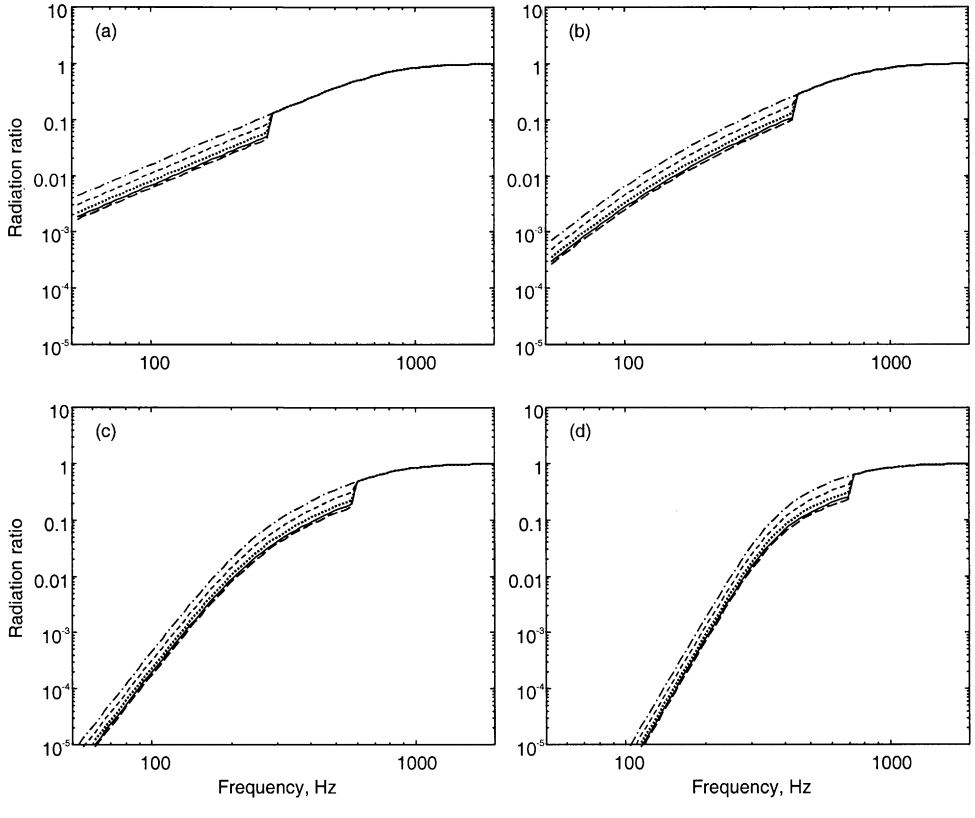

Figure 16. Approximate radiation ratios of radial motion for various straight-webbed wheels with radius 0.42 m. ——, normal wheel; – – –, double thickness tyre; ·····, half-thickness tyre; –· – ·, solid web; - - - wide web. (a) $n = 0$, (b) $n = 1$, (c) $n = 2$, (d) $n = 3$.

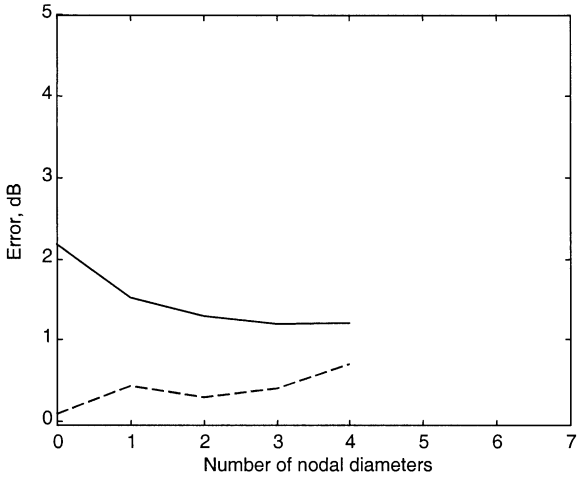

Figure 17. Error in radiation index of radial motion if equations (6), (7) and (9) are used. ——, r.m.s. error for all frequency points in range, – – –, mean error.

The curves shown in Figure 9 are based on equations (6)–(8), with the transition frequencies f_{r1}, f_{r2} and f_{r3} given above factored by $(r/0{\cdot}42)^{-1/2}$:

$$f_{r1} = 120n/(r/0{\cdot}42)^{1/2}, \quad f_{r2} = 800/(r/0{\cdot}42)^{1/2}, \quad f_{r3} = (280 + 150n)/(r/0{\cdot}42)^{1/2}. \qquad (9a-c)$$

Figure 17 shows the r.m.s. difference between the results from these simple formulae and the BE results, which are only available for $n \leqslant 4$. These differences are averaged over the results for four different radii and the four different web/tyre geometries. Apart from $n = 0$, where large discrepancies are present below 200 Hz, the results show reasonable agreement.

5. DIRECTIVITY OF WHEEL RADIATION

The results so far have concentrated on the radiation ratio, which allows the sound power to be predicted from a knowledge of the vibration amplitude and distribution. To obtain the sound pressure at a given point in the far field, the directivity of the sound field is also required.

In practice, the noise due to a wheel is usually observed at a position that is fixed relative to the ground as the train passes, and the quantity of interest is an average sound level due to the train rather than the precise time-varying sound pressure level. A similar consideration applies for interior noise, since the airborne sound transmission to the interior is determined by the overall sound field in a region under the vehicle rather than the sound pressure at any particular location under the floor. Moreover, the directivity of the noise from a wheel will be affected by local geometric features such as the bogie frame and vehicle body. For these reasons, the detailed directivity is of little practical relevance. It is sufficient to obtain an indication of the approximate nature of the directivity.

Measurements are presented in reference [17] of the sound field around each of five different types of railway wheel, excited at their natural frequencies. In each case microphones were located around a semi-circular frame of radius 1·5 m, centred at the centre of the wheel. The wheel was excited radially on the tyre, on the opposite side to the

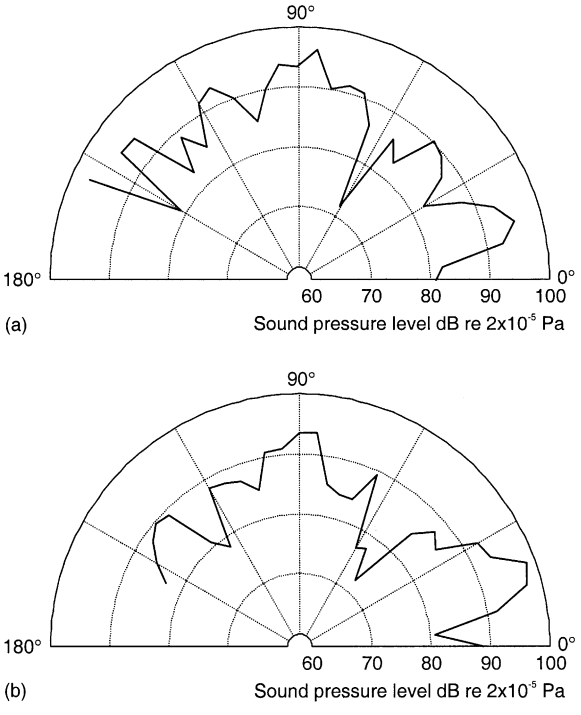

Figure 18. Sound pressure normalized to input force around an NS Intercity wheel for radial modes. The wheel axis lies at the angle 0°, angles greater than 90° represent positions behind the wheel. (a) $n = 3$, 2470 Hz; (b) $n = 5$, 4060 Hz [17].

microphones, by repeated impacts. Measurements were presented in terms of the sound pressure normalized to the input force rather than the directivity as such.

Example results are shown in Figures 18 and 19 for an NS Intercity 920 mm diameter wheel, for 1-nodal-circle and radial modes respectively. This wheel has a straight web so that its radial and axial motions are less well coupled than those of the freight wheel shown in Figure 1 [17]. Although the results are rather complex, it can be seen that the sound pressure for the radial modes has a similar level around the semi-circular arc, whereas the axial modes have a lower sound pressure above the wheel tread (90°) than in the axial direction (0°). The sound pressure was generally found to have a minimum on or close to the axis of the wheel for both types of mode, due to cancellation between the contributions from different parts of the mode shape; a maximum was obtained for $n = 0$ [17].

Results in reference [17] for wheels with a curved web resembled the radial mode results of Figure 18, since the predominantly axial modes also contain radial motion.

In seeking a simple model to represent the overall behaviour seen in Figures 18 and 19, a distinction is made between axial and radial motion. For radial motion the sound field can be closely approximated by an omni-directional field, whereas for the axial motion a dipole distribution is more appropriate since this has a maximum in the axial direction and a minimum in the plane of the wheel. Such results are shown in Figure 20.

6. CONCLUDING REMARKS

The radiation ratio of a railway wheel vibrating in various mode shapes has been obtained from boundary element calculations. Simple parametric models have been

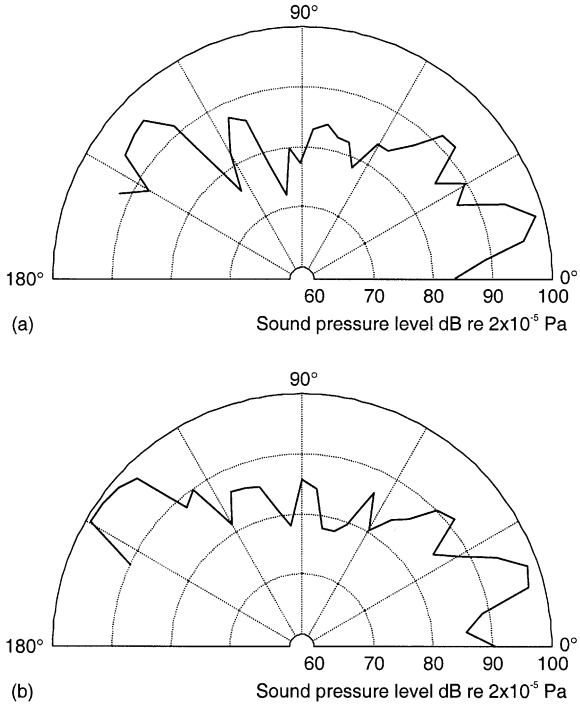

Figure 19. Sound pressure normalized to input force around an NS Intercity wheel for 1-nodal-circle axial modes. The wheel axis lies at the angle 0°, angles greater than 90° represent positions behind the wheel. (a) $n = 3$, 2740 Hz; (b) $n = 5$, 3850 Hz [17].

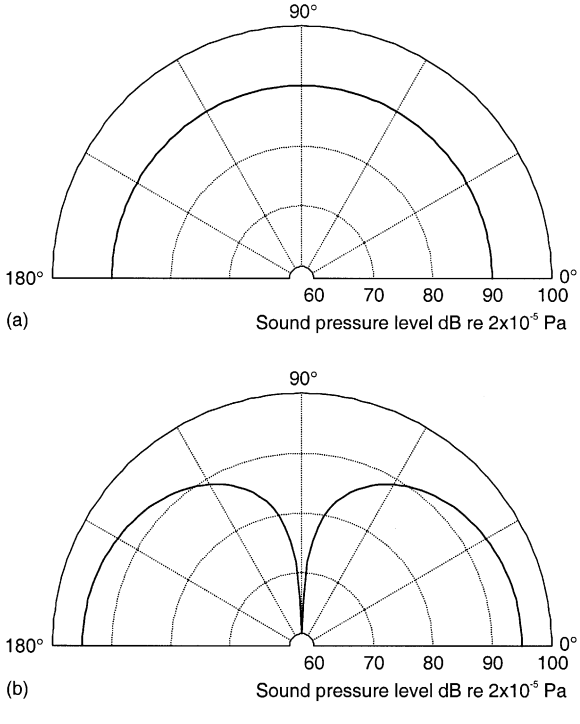

Figure 20. Sound pressure distribution for (a) monopole-type source, (b) dipole-type source.

established from these results for the radiation ratios of axial and radial motion, showing the dependence on the number of nodal diameters, the wheel radius, and other geometric features. These formulae are much more efficient than full boundary element predictions and depend only on a few simple geometric parameters. They have been included in the latest versions of the TWINS program (Track–Wheel Interaction Noise Software) for predicting railway rolling noise [5, 6]. Similarly, the directivity is based on a dipole distribution for axial motion and a monopole (omni-directional) distribution for radial motion.

ACKNOWLEDGMENTS

The boundary element predictions were performed by Thomas Bruneteau, a visiting student from ENSIL, Limoges in France. Part of the work described here was carried out within the EU Brite Euram project "Silent Freight", project number BE 95-1238. The measurements of radiation ratio were performed by TNO Institute of Applied Physics in the Netherlands as part of the "Silent Freight" project; in particular the assistance of Lau Hopmans and Marcel Janssens is gratefully acknowledged.

REFERENCES

1. D. J. Thompson, C. J. C. Jones 2000 *Journal of Sound and Vibration* **231**, 519–536. A review of the modelling of wheel/rail noise generation.
2. P. J. Remington 1976 *Journal of Sound and Vibration* **46**, 359–379. Wheel/rail noise. Part I: characterization of the wheel/rail dynamic system.
3. P. J. Remington 1976 *Journal of Sound and Vibration* **46**, 419–436. Wheel/rail noise. Part IV: rolling noise.
4. P. J. Remington 1987 *Journal of the Acoustical Society of America* **81**, 1805–1823. Wheel/rail rolling noise, I: theoretical analysis.
5. D. J. Thompson, B. Hemsworth and N. Vincent 1996 *Journal of Sound and Vibration* **193**, 123–135. Experimental validation of the TWINS prediction program for rolling noise. Part 1: description of the model and method.
6. D. J. Thompson, P. Fodiman and H. Mahé 1996 *Journal of Sound and Vibration* **193**, 137–147. Experimental validation of the TWINS prediction program for rolling noise. Part 2: results.
7. D. J. Thompson 1993 *Journal of Sound and Vibration* **161**, 401–419. Wheel–rail noise generation. Part II: wheel vibration.
8. J. W. Strutt (Lord Rayleigh) 1896 *Theory of Sound*. New York: Dover Publications; second edition, 1945 re-issue. See section 278.
9. G. Maidanik 1962 *Journal of the Acoustical Society of America* **34**, 809–826 (Erratum in **57** (1975) 1552). Response of ribbed panels to reverberant acoustic fields.
10. C. E. Wallace 1972 *Journal of the Acoustical Society of America* **51**, 946–852. Radiation resistance of a rectangular panel.
11. E. Schneider, K. Popp and H. Irretier 1988 *Journal of Sound and Vibration* **120**, 227–244. Noise generation in railway wheels due to rail–wheel forces.
12. D. J. Thompson 1988 *Journal of Sound and Vibration* **120**, 275–280. Predictions of acoustic radiation from vibrating wheels and rails.
13. U. Fingberg 1990 *VDI Fortschritt-berichte*, Reihe 11, Nr. 140. Ein Modell für das Kurvenquietschen von Schienenfahrzeugen.
14. A. H. W. M. Kuijpers, G. Verbeek and J. W. Verheij 1997 *Journal of the Acoustical Society of America* **102**, 1394–1401. An improved acoustic Fourier boundary element method formulation using fast Fourier transform integration.

15. N. VLAHPOULOS 2000 in *Boudary Element Acoustics: Fundamentals and Computer Codes* (T. W. WU, editor). Southampton: WIT Press. Indirect variational boundary element method in acoustics.
16. L. J. M. HOPMANS 1997 *TNO Memorandum HAG-MEMO*-97-0108 (issued within Silent Freight project). Wheel radiation efficiency measurements.
17. D. J. THOMPSON and M. G. DITTRICH 1991 *ORE Technical Document DT*248 (*C*163), *Utrecht.* Wheel response and radiation—laboratory measurements of five types of wheel and comparisons with theory.